Journal of Enhanced Heat Transfer, 27(2):123–141 (2020)

GENETIC ALGORITHM MULTIOBJECTIVE OPTIMIZATION OF A THERMAL SYSTEM WITH THREE HEAT TRANSFER ENHANCEMENT CHARACTERISTICS

***Reza Beigzadeh*[1,*] *& Smith Eiamsa-ard*[2]**

[1]*Department of Chemical Engineering, Faculty of Engineering, University of Kurdistan, Sanandaj, Iran*

[2]*Department of Mechanical Engineering, Faculty of Engineering, Mahanakorn University of Technology, Bangkok 10530, Thailand*

*Address all correspondence to: Reza Beigzadeh, Department of Chemical Engineering, Faculty of Engineering, University of Kurdistan, Sanandaj, Iran; Tel.: +98 918 836 8042; Fax: +98 873 366 8513, E-mail: r.beigzadeh@uok.ac.ir

Original Manuscript Submitted: 9/30/2019; Final Draft Received: 11/23/2019

A heat transfer enhancement system including CuO/water nanofluid in a corrugated tube equipped with twisted tape was modeled by two well-known artificial neural network techniques. The multilayer perceptron and group method of data handling neural networks were employed to predict thermal-hydraulic characteristics as functions of main operating conditions. In addition, the genetic algorithm (GA) approach was used to develop applied empirical correlations. The purpose of the models is to estimate Nusselt number (Nu) and friction factor (f) in the investigated heat exchanger. The main effective parameters investigated in this study are volume fraction of nanoparticle, twist ratios of twisted tape, and Reynolds number. According to the conflicting relationship between heat transfer and pressure drop, the more accurate model was selected as the objective functions for multiobjective optimization by GA. The optimum operating conditions of the investigated heat exchangers that lead to a trade-off between Nu and f were proposed.

KEY WORDS: *optimization, genetic algorithms, neural network, heat transfer enhancement, nanofluid, tube insert*

1. INTRODUCTION

Heat transfer enhancement (HTE) approaches are highly regarded due to the importance of optimizing energy consumption. In general, HTE is divided into two methods: active and passive. Some significant cases of passive methods include employing nanofluids or tube inserts, and roughening channel surfaces. These methods are usually accompanied by undesirable effects like increasing pressure drop along with enhancing heat transfer. Therefore, developing accurate and reliable models for predicting heat transfer and pressure drop in HTE systems are very suitable to optimize heat exchangers. The literature review shows the great capability of artificial neural networks (ANNs) to model and predict target variables in heat transfer systems (Ali et al., 2015; Mohanraj et al., 2015). Tube inserts cause a significant augmentation in heat transfer rate

NOMENCLATURE

A	coefficient or weight vectors	W	weight
A_i	inner heat transfer surface area (m^2)	w	twisted tape width (m)
b	bias	Y	ultimate output
c_p	specific heat capacity of fluid (J/kg K)	y	neuron output/Twist length (m)
d	diameter of the corrugated tube (m)	**Greek Symbols**	
f	friction factor	φ	volume fraction of nanoparticle
F	transfer function	μ	dynamic viscosity (Pa s)
h	heat transfer coefficient (W/m^2 K)	ρ	density (kg/m^3)
k	thermal conductivity (W/m K)	μ	fluid dynamic viscosity (kg/s m)
L	length of the test section (m)		
$\dot{m}$	mass flow rate (kg/s)		
N	number of data	**Subscripts**	
Nu	Nusselt number	f	base fluid
p	predicted data	i	input layer/inner
ΔP	pressure drop (Pa)	in	inlet
Re	Reynolds number	j	hidden layer
r	real data	k	output layer
T	temperature (K)	n	nanofluid
U	overall heat transfer coefficient	out	outlet
V	velocity (m/s)	p	nanoparticle

through the formation of swirling flows and increase the turbulence intensity near the tube wall. The effects of different tube inserts on heat transfer coefficient and turbulence intensity have been investigated in several studies during the past two decades (Ali et al., 2015; Boulahia et al., 2017; Piriyarungrod et al., 2018; Shabanian et al., 2011). Jafari Nasr et al. (2010) examined the capability of the ANN to model the thermal and flow data related to helical wire coil inserts. The empirically obtained data of the four wire coil inserts were employed for developing the prediction model. Moreover, the precision of the developed ANNs was compared with power-law correlations. The results indicate the higher prediction accuracy of the ANN in comparison with empirical correlations. Zheng et al. (2017) performed a numerical analysis to study the heat transfer and hydraulic characteristics in tubes equipped with vortex rod inserts. The optimum parameters have been obtained using the ANN and genetic algorithm (GA) multiobjective optimization method. Beigzadeh et al. (2014) applied the ANN and GA to model the heat transfer performance in a channel with twisted tape vortex generators.

Using the nanofluid as an HTE procedure in the heat transfer equipment has recently been frequently considered in experimental and numerical literature (Abdollahi-Moghaddam et al., 2018; Baghban et al., 2019; Ghahdarijani et al., 2017). The nanofluids are the fluids with nanometer-sized particles that can have more heat transfer coefficients compared to the base fluid.

Nanofluids are employed in various applications such as automotive radiators to obtain improved thermal performance (Molana, 2017), electronics cooling (Bahiraei and Heshmatian, 2018), and mixed convection in enclosures (Izadi et al., 2018). Al-Rashed et al. (2019) investigated the geometry effects of nanofluids in a wavy-walled microchannel heat sink. Nagaraj (2019) provided a literature review about numerical and empirical research on the thermal performance in microchannels for different nanofluids.

Recently, Guo (2020) provided a comprehensive review on HTE with use of nanofluids, in which the progress of ANN in nanofluid research was emphasized. Heat transfer improvement of Al_2O_3-water nanofluid in microchannels was numerically investigated by Nandakrishnan et al. (2018). Pal and Bhattacharyya (2018) used a single-phase model to study the nanofluid flow and thermal characteristics in a channel with a blunt ribs wall. They show that multiple numbers of ribs led to an enhanced thermal performance but reduced heat transfer compared to a single rib. Fard et al. (2019) investigated the effects of carbon nanotubes and water as working fluid on flow and heat transfer characteristics in coiled tubes.

The neural networks can be applied for estimating thermal characteristics in these systems as functions of main operating conditions such as the concentration of nanofluid. Abdollahi-Moghaddam et al. (2018) investigated the effects of CuO/water nanofluid concentrations on heat transfer and pressure drop inside a horizontal tube. The experimental data were used for developing an ANN to predict Nusselt number (Nu) in the heat exchanger. The suggested network involves one hidden layer and eight hidden neurons. The numerical modeling of a helically coiled heat exchanger was performed by Baghban et al. (2019). The water carbon nanofluid was used as the working fluid. They examined the ANN, adaptive neurofuzzy inference system, and least squares support vector machine (LSSVM) for modeling. The research demonstrates that the LSSVM has the best prediction precision for the studied system. Mohammadi Ghahdarijani et al. (2017) applied the ANN to estimate the performance of a reactor cooling jacket with aqueous Al_2O_3 and CuO nanofluids.

The roughening of the tube's inside surfaces leads to increasing heat transfer area. Moreover, this method makes secondary flows, which lead to an increase of turbulence intensity as well as heat transfer coefficient. The combination of corrugated tubes and tube inserts as two HTE methods were investigated in the literature (Nasr and Khalaj, 2010; Zimparov, 2001). Zimparov (2001) investigated the thermal and flow characteristics in spirally corrugated tubes equipped with twisted tape inserts. Spirally ribbed channels and twisted tape inserts with various geometries were investigated experimentally. Nasr and Khalaj (2010) proposed ANNs for modeling a heat exchanger including corrugated tubes equipped with twisted tape inserts. The related experimental data (Zimparov, 2004a,b) was used for modeling procedures. The model input variables were geometrical parameters and Reynolds number (Re) and the targets are friction factor (f) and Nu.

Very high heat transfer coefficients can be obtained using a combination of the three mentioned HTE methods including tube insert, nanofluid, and corrugated tube. However, it was noted that all the HTE methods can lead to a further pressure loss in the heat exchanger and also higher required pumping power. In this investigation, the ANN and GA approaches were used for modeling heat transfer and pressure drop characteristics in the heat exchanger in which all three HTE methods have been used. The ability of well-known ANNs, including the multilayer perceptron (MLP) and group method of data handling (GMDH) was challenged. The input parameters were volume fraction of nanoparticle, twist ratios of twisted tape, and Re, and the output variables were Nu and f. The nonlinear dependence between the input-output variables indicated that the ANNs can be suitable models to solve the problem. The applied data points for determining the

precise model were obtained from experimental work. The reliable developed model was introduced as the objective functions of the GA multiobjective optimization procedure. Finally, the optimum parameters were proposed for designing the efficient thermal system.

2. METHODOLOGY

2.1 Experimental Procedure and Data Collection

An experimental setup was applied to investigate the benefits of the tube inserts, corrugated tube, and nanofluid on heat transfer improvement. The related flow diagram and experimental apparatus are schematically illustrated in Fig. 1. The main setup apparatus include a heat exchanger with concentric tubes; cold and hot water tank; centrifugal pumps; variac transformer; and temperature, pressure, and flow measuring devices including thermocouple, manometer, and rotameter, respectively. The hot and cold fluid flowing was passed through the tube and shell, respectively, and the heat transfer coefficients and pressure drops were measured in different operating conditions. The details related to the experimental procedure have been explained in previous work (Wongcharee and Eiamsa-ard, 2012).

The experiments have been carried out on three tube inserts inside a corrugated tube. The aluminum twisted tapes with a thickness of 0.8 mm and length of 900 mm were employed in the experiments. A twisted tape width (w) of 9 mm and three twist lengths (y) of 24 mm, 32 mm, and 48 mm were investigated. The twist lengths (y) are related to twist ratios (y/w) of 2.7, 3.6, and 5.3, respectively. The geometrical parameters of w and y were illustrated in Fig. 1. The studied tube inserts were placed in a stainless steel corrugated tube with 1 mm wall thickness and an inner diameter of 10 mm.

The heat transferred by cold or hot fluids can be obtained as follows:

$$Q = \dot{m} c_p (T_{in} - T_{out}) \tag{1}$$

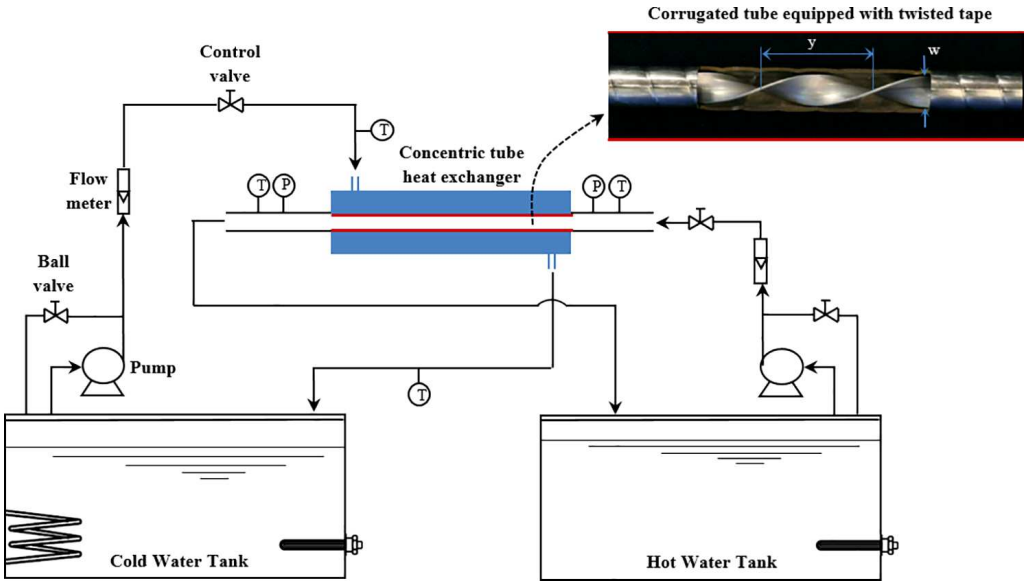

FIG. 1: Flow diagram of the experimental setup

in which $\dot{m}$ is mass flow rate and c_p is specific heat capacity of fluid. The average heat transfer rate of heat and cold fluid was considered in the calculations. The overall heat transfer coefficient (U) can be calculated from

$$Q = UA_i\Delta T_{LMTD} \tag{2}$$

The inner heat transfer coefficient (h_i) was obtained from the overall heat transfer coefficient as follows:

$$\frac{1}{U} = \frac{1}{h_i} + \frac{A_i \ln(d_o - d_i)}{2\pi kL} + \frac{A_i}{A_o h_o} + R_f \tag{3}$$

When the last three terms on the right side of Eq. (3) were considered constant the equation becomes

$$\frac{1}{U} = \frac{1}{h_i} + B \tag{4}$$

The relation between Re and heat transfer coefficient is

$$h_i = C\mathrm{Re}^m \tag{5}$$

so,

$$\frac{1}{U} = \frac{1}{C\mathrm{Re}^m} + B = A\mathrm{Re}^{-m} + b \tag{6}$$

This equation indicates that the plot between $1/U$ and Re^{-m} leads to a straight line with the slope of A and intercept at B in $1/U$ axis. From Eqs. (5) and (6), the following equation is obtained:

$$h_i = \frac{1}{1/U - B} \tag{7}$$

The Nu of the flow in the tube is calculated as follows:

$$\mathrm{Nu} = \frac{h_i d_i}{k} \tag{8}$$

in which d_i is the diameter of the corrugated tube and k is thermal conductivity of fluid.

In addition, Re and f were calculated using the following equations:

$$\mathrm{Re} = \frac{\rho V d_i}{\mu} \tag{9}$$

$$f = \frac{2\Delta P d_i}{\rho V^2 L} \tag{10}$$

in which ρ is fluid density, μ is dynamic viscosity, ΔP is pressure drop, L is length of the test section, and V is mean axial flow velocity.

CuO-water nanofluids with volume fractions (φ) of 0.3%, 0.5%, and 0.7% were prepared to examine the effects of nanofluid concentration on heat transfer improvement. The mixture properties for CuO-water nanofluid were calculated using the following relations:

$$\rho_n = \varphi\rho_p + (1 - \varphi)\rho_f \tag{11}$$

- Density:

  in which the subscripts of n, p, and f refer to the nanofluid, nanoparticle, and base fluid (water), respectively.

- Specific heat capacity (Pak and Cho, 1998):

$$(\rho C_p)_n = \varphi(\rho C_p)_p + (1-\varphi)(\rho C_p)_f \tag{12}$$

- Thermal conductivity (Vajjha et al., 2010):

$$\frac{k_n}{k_f} = \frac{k_p + 2k_f + 2\varphi(k_p - k_f)}{k_p + 2k_f - \varphi(k_p - k_f)} \tag{13}$$

- Dynamic viscosity (Einstein, 1911):

$$\mu_n = \mu_f(1 + 2.5\phi) \tag{14}$$

2.2 Developing Prediction Models

The basis of the neural networks is the imitation of the interconnected structure of brain cells in order to model complex systems. This research attempted to compare two well-known ANNs including MLP and GMDH to model a heat exchanger with three HTE options. The main effective parameters of the heat exchanger are volume fraction of nanoparticles (φ), twist ratios of the twisted tapes (y/w), and Re. These variables were used as the input data for developing the models. The important features in the heat exchangers are the heat transfer and pressure drop characteristics. The improvement in heat transfer coefficients is usually associated with a growth in pressure drop and more energy is required for the fluid pumping. Therefore, two thermal and hydraulic characteristics in the investigated heat transfer system including Nu and f were selected as output data of the models. Separate models were considered for estimating Nu and f to achieve more accurate models. The model validity should be proved using data points that were not employed for training. Hence, a third of the used data was employed to validate the ANNs and the rest was applied to develop the models. A total of 132 empirical data points were prepared for training and validating the MLP and GMDH neural networks. The range of the input and output variables was tabulated in Table 1. The following deviation equations were used for evaluation of the precision of the provided models:

$$\text{MRE}(\%) = \frac{100}{N}\sum_{i=1}^{N}\left(\frac{|r_i - p_i|}{r_i}\right) \tag{15}$$

$$\text{MSE} = \frac{1}{N}\sum_{i=1}^{N}(r_i - p_i)^2 \tag{16}$$

TABLE 1: The range of the used variables

Variable	Minimum	Maximum
Nu	61.37	287.69
f	0.12048	0.30246
Re	6259.4	24264.4
φ (%)	0	0.7
y/w	2.7	5.3

in which MRE and MSE represent the mean relative error and mean squared error, respectively. N is the number of all data, p is the predicted data by the model, and r is the real (target) data.

In addition, due to the ease of use of empirical correlations, two power-law equations were created using GA to compare with the neural network models.

2.2.1 MLP Neural Network

The ability of the MLP neural networks to recognize the nonlinear and complex problems encouraged many researchers to apply it for modeling (Ali et al., 2015). The structural design of the MLP neural network consists of three main layers including input, hidden, and output layer. The layers arranged with simple processing elements are named as node or neuron. The MLP-ANN parameters are obtained using the back propagation algorithm. The information related to the input layer is fed forward recursively toward the hidden layer and then is delivered toward the output layer. The MSE between the network response and target values is calculated at the network output and is returned backward to correct the ANN parameters. More hidden layers and hidden neurons lead to complexity of the ANN and it can cause overfitting of the model. Therefore, in the work, the MLP-ANN with three layers that contain a hidden layer was developed. The number of neurons in the hidden layer was optimized by trial and error. In the mentioned procedure, the effectiveness of the ANN is assessed for the different number of hidden neurons and the most proper number is selected.

In the structure of the MLP network, all neurons are interconnected and the information is transferred between the layers. The output of each neuron and the final output of the model is calculated as follows:

$$y_j = F_t\left(\sum_{i=1}^{m} W_{j\,i} X_i + b_j\right) \tag{17}$$

$$Y = F_p\left\{\sum_{j=1}^{n} W_{k\,j}\left[F_t\left(\sum_{i=1}^{m} W_{j\,i} X_i + b_j\right)\right] + b_k\right\} \tag{18}$$

$$F_t(x) = \frac{e^x - e^{-x}}{e^x + e^{-x}} \tag{19}$$

$$F_p(x) = x \tag{20}$$

in which y_j is the output from jth neuron, Y is the ultimate output of the MLP-ANN, X is ANN input, and W and b are the model parameters (weights and biases). The n and m are the number of neurons and the number of input variables, respectively. The subscripts i, j, and k refer to the input, hidden, and output layer, respectively. F_t and F_p are the hyperbolic tangent sigmoid and linear transfer functions, respectively, that are applied to obtain a normalized output from each neuron. All employed data is normalized between zero and one to improve the computational process.

2.2.2 GMDH Neural Network

The GMDH is a polynomial artificial neural network, which used the inductive self-organizing approach to model the typically complex systems. The GMDH with simpler interconnections between layers and a programmed algorithm to structure design was originally presented by Ivakhnenko (1971). The structure of the GMDH consists of several interconnected layers and

neurons. The output is calculated based on the Volterra–Kolmogorov–Gabor polynomial equation:

$$Y(x_1, ..., x_n) = a_0 + \sum_{i=1}^{n} a_i x_i + \sum_{i=1}^{n}\sum_{j=1}^{n} a_{ij} x_i x_j + \sum_{i=1}^{n}\sum_{j=1}^{n}\sum_{k=1}^{n} a_{ijk} x_i x_j x_k + ... \tag{21}$$

where $X(x_1, x_2, ..., x_n)$ are the input variable vectors, $A(a_1, a_2, ..., a_R)$ are the coefficient or weight vectors, and a_0 is the neuron bias. Generally, in the model structure, each neuron has five weights and one bias. In the case of the GMDH in which the neurons have two inputs, a polynomial of maximum order two was used:

$$y(x_i,x_j) = a_0 + a_1 x_i + a_2 x_j + a_3 x_i x_j + a_4 x_i^2 + a_5 x_j^2 \tag{22}$$

where y is neuron output. Actually, the considered neuron output of the MLP and GMDH neural networks [Eqs. (17) and (22)] expressed the ultimate relationship between the output-input variables. The constants of the equation or weights are obtained using least square regression approaches (Ahmadi et al., 2015):

$$E = \sum_{i}^{M} (y_i - r_i)/N \rightarrow \min \tag{23}$$

in which y_i and r_i are real and predicted values, respectively. N is the number of data.

In the GMDH structure, the input variables are considered the first layer of the network. Since each neuron of the next layers has two inputs, the [m × (m − 1)/2] neurons are generated in the second layer in which m is the number of variables. After determining the output of the neurons [Eq. (22)] using regression methods, the neurons with higher precision are selected and the weaker neurons are removed. This procedure is similar to the principle of evolution. The output of the neurons is inserted as the input of neurons in the next layer, which makes a multilayer arrangement. The MSEs of the neurons in each layer are compared with the previous layer. If the deviation values in the new layer are more than the earlier layer, the addition of layers is stopped. Finally, the neuron with higher accuracy is determined as the ultimate output of the GMDH-ANN (Fujimoto and Nakabayashi, 2003).

2.2.3 GA-Based Correlations

The search method is based on the GA inspired by Darwinian survival law and widely used in engineering optimization problems (Mohanraj et al., 2015). The optimization process starts with an initial random population (answers) and the generation continued by processes including parent selection, elitism, crossover, mutation, and replacement. The iterative evolution procedure continues until the desired response is obtained.

The following functional relationships are considered to develop two correlations between the Nu and f as functions of Re, twist ratios of twisted tape (y/w), and volume fraction of nanoparticle (φ):

$$\mathrm{Nu} = C_1 \mathrm{Re}^{C_2} \left(\frac{y}{w}\right)^{C_3} (1+\phi)^{C_4} \tag{24}$$

$$f = C_1' \mathrm{Re}^{C_2'} \left(\frac{y}{w}\right)^{C_3'} (1+\phi)^{C_4'} \tag{25}$$

The MSE is employed as the objective function of the GA optimization to obtain optimum correlation constants (C_i and C_i') as follows:

$$\mathrm{MSE}_{\mathrm{Nu}}(C_1, C_2, C_3, C_4) = \frac{1}{N}\sum_{i=1}^{N}\left(\mathrm{Nu}_i^{Exp} - \mathrm{Nu}_i^{\mathrm{Pred}}\right)^2 \tag{26}$$

$$\mathrm{MSE}_f(C_1', C_2', C_3', C_4') = \frac{1}{N}\sum_{i=1}^{N}\left(f_i^{Exp} - f_i^{\mathrm{Pred}}\right)^2 \tag{27}$$

The GA procedure attempts to minimize the above objective functions. The important details related to the used GA such as initial population, crossover fraction, elite children, and generations are reported in Table 2.

2.3 GA Multiobjective Optimization

In single-objective optimization, a system with one target variable was considered for optimum designing. However, in real engineering equipment, there are many design factors that need trade-offs among them. The target factors are usually conflicted with each other, and the multiobjective optimization is employed with respect to all objectives. Pareto solutions are a set of answers for a multiobjective problem. Several practical engineering problems involve detecting the minimum or maximum of multiple objectives simultaneously. There is no single solution to optimize multiple goals at once, therefore in multiobjective optimization, the target is to obtain a set of nondominated answers known as Pareto optimal solutions. The GA is a global optimization procedure, which is appropriate to search the different Pareto optimum solutions for solving multiobjective optimization problems. Multiobjective GA optimization has more abilities than the classical techniques in terms of the optimizing problems in which the objective functions are nonlinear, nondifferential, or discontinuous (Konak et al., 2006; Sanaye and Dehghandokht, 2011).

In the study, the GA was used to determine the Pareto set related to the heat transfer and pressure drop in a heat exchanger including tube insert and nanofluid. The multiobjective optimization based on GA was applied to find optimum parameters (Re, y/w, and φ) in the investigated thermal system, which led to the minimizing pressure drop (pump power) and the maximizing heat transfer rate. Regarding objective functions that are minimized in the GA multiobjective optimization, the following forms of the equations were considered objectives:

$$\mathrm{OF}_1\left(\mathrm{Re}, \frac{y}{w}, \phi\right) = \frac{1}{1+\mathrm{Nu}} \tag{28}$$

$$\mathrm{OF}_2\left(\mathrm{Re}, \frac{y}{w}, \phi\right) = f \tag{29}$$

TABLE 2: Details of the genetic algorithm optimization method

Number of initial population chromosomes	100
Crossover fraction	0.8
Number of elite children	2
Number of generations	300

The procedure was carried out by 400 generations and the initial population number was 100 chromosomes. The optimization process terminates once the number of generation reaches the ultimate value.

3. RESULTS AND DISCUSSION

The main characteristics of a heat exchanger that benefits from HTE options including tube insert, corrugated tube, and nanofluid were modeled using two powerful models. The ability of two subcategories of ANNs, MLP and GMDH, were investigated to predict Nu and f in the heat exchanger. A data set that includes 132 experimental data was gathered and divided into two parts for training and validating the models. To assess the model validation, all 132 data points were randomly divided into two groups. The first data section (two-thirds of data points) was used to train the models and the second data section (remaining data) was applied to validate the developed models. This procedure leads to minimizing the chances to have a biased data set and increases the chances to have a representative data set for the training data.

The volume fraction of nanoparticles of $\varphi = 0.7\%$, 0.5%, and 0.3%; twist ratios of the twisted tapes of $y/w = 5.3$, 3.6, and 2.7; and Re range of Re = 6259–24,264 were employed as input data for modeling. Changing the mentioned operating conditions led to simultaneous variations in heat transfer rate and friction characteristics in the investigated system. The detailed experimental analysis related to the effects of the investigated variables on the heat exchanger in which it was expressed (Wongcharee and Eiamsa-ard, 2012). The accurate model provides the possibility to choose optimal conditions. In the present study, two MLP and also two GMDH neural networks were developed to evaluate Nu and f in the studied heat exchanger. Finally, the more accurate model for predicting Nu and f was used for appropriate objective functions in a multiobjective GA optimization. The detailed results related to the models are explained in subsequent sections.

3.1 MLP-ANN Results

Figure 2 shows the arrangement of the MLP-ANN architecture that includes the input, hidden, and output layers. The various structures of the MLP-ANN were examined to acquire the best model via the trial-and-error approach. The resulted MSE for the various numbers of neurons of the hidden layer was presented in Fig. 3. According to the figure, the ANNs with eight and nine neurons were selected as optimum networks for predicting the Nu and f, respectively. The MRE and MSE of 0.196% and 0.111, respectively, were calculated for the Nu model, and the values of 0.063% and 3.97×10^{-8} were obtained for the f model, respectively. In addition, the deviations of the test data set were calculated and the MRE values of 0.169% and 0.04% were obtained for prediction of Nu and f, respectively. The ability of the developed model to estimate the test data and also the reasonable difference between deviations of the predicted train and test data set proved the validity of the model. The performance of other algorithms for training the MLP-ANN was evaluated and the error values were reported in Table 3. The similar modeling procedure was carried out to specify the model structure such as the optimum number of hidden neurons. The results indicate the superiority of the Levenberg–Marquardt algorithm in comparison to other learning algorithms. The obtained parameters of the MLP neural networks were tabulated in Tables 4 and 5. The reported weights and biases (W, b) should be inserted in Eq. (18) to obtain the predicted output of the models. The data points were normalized before the modeling process; the real output can be found using the following relation:

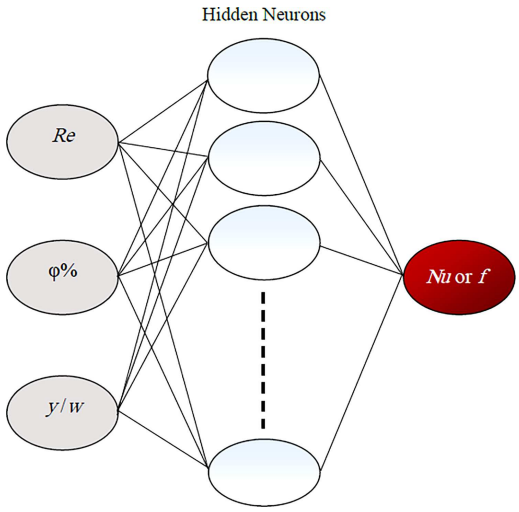

FIG. 2: Structure of the MLP-ANN

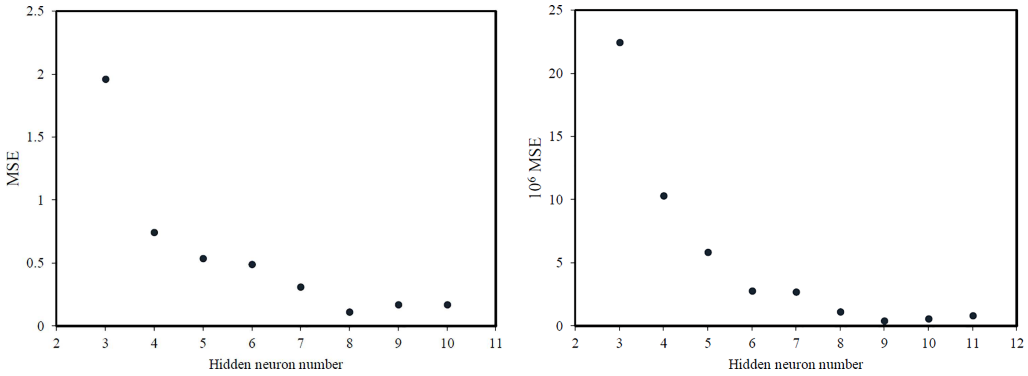

FIG. 3: Deviations of the MLP-ANNs versus the number of neurons in the hidden layer for prediction of (a) Nu and (b) f

$$\text{Real value} = [\text{Normalized data}(\text{Maximum value} - \text{Minimum value})] + \text{Minimum value} \quad (30)$$

in which the maximum and minimum values were reported in Table 1.

3.2 GMDH-ANN Results

In the present work, two GMDH-Type-ANN were developed to estimate target variables (Nu and f) based on empirical data. Figure 4 shows the two structures related to the developed GMDH neural networks for predicting Nu and f. These arrangements were optimized to predict the target data with high precision. As can be seen in Fig. 4, both structures contain two hidden layers. The related genome representations of the developed models for estimating Nu and f are $x_1x_3x_1x_1x_2x_3x_1x_1$ and $x_1x_2x_3x_3x_2x_3x_1x_1$, respectively, where x_1, x_2, and x_3 placed for Reynolds

TABLE 3: Evaluation of the different training algorithms for modeling the Nu and f

Training algorithm	Nu		f	
	Number of optimum hidden neurons	MRE (%)	Number of optimum hidden neurons	MRE (%)
Levenberg–Marquardt	8	0.196	9	0.063
Conjugate gradient back propagation with Powell–Beale restarts	6	2.71	9	3.41
Bayesian regularization back-propagation	6	14.41	8	18.39
Batch training with weight and bias learning rules	7	1.24	8	1.17
Gradient descent with adaptive learning rate back propagation	7	10.51	9	7.92
Gradient descent with momentum back propagation	5	17.39	8	17.71

TABLE 4: The MLP-ANN parameters for prediction of Nusselt number

Neuron	W_{ji}	—	—	b_j	$b_k = 0.7108$
—	Re	φ (%)	y/w	—	W_{kj}
1	–1.0191	4.7141	–4.6180	0.9495	–0.0176
2	–0.2997	4.1446	4.5960	–4.7741	–0.0327
3	0.8172	0.4517	–0.2901	–1.1104	0.5949
4	2.4987	1.6162	–2.5877	–3.9685	0.0728
5	0.2668	–0.5915	–4.1661	–0.3853	0.1397
6	1.2074	0.1915	0.0390	–0.1383	0.2769
7	–3.6278	–1.2430	5.3412	0.2888	0.0035
8	3.0564	–0.5738	2.0421	0.1483	0.0322

number (Re), volume fraction of nanoparticle (φ), and twist ratios of twisted tape (y/w), respectively. The polynomial expression of the GMDH-ANNs is shown in Tables 6 and 7. These polynomial relations can be used for estimating the Nu and f as a function of input variables. The MRE values of all predicted data points were obtained as 0.718% and 1.309% for Nu and f models, respectively. In addition, the MREs of 0.780% and 1.39% were calculated for the test data set. Therefore, the modeling procedure and presented models are validated to predict the output variables.

3.3 GA-Based Correlations

Two classical power-law correlations [Eqs. (24) and (25)] were considered to estimate target variables (Nu and f) due to the availability and high usage speed. The GA search technique was

TABLE 5: The MLP-ANN parameters for prediction of friction factor

Neuron	W_{ji}	—	—	b_j	$b_k = 0.7301$
—	**Re**	**φ (%)**	y/w	—	W_{kj}
1	2.3705	–3.1972	–0.7069	–2.1029	0.0511
2	–0.1367	11.2831	–2.2876	–7.9671	0.0687
3	–3.2383	1.8736	0.3915	1.4413	–0.0190
4	–3.8067	–0.4611	–2.4525	2.7763	0.0137
5	1.4123	0.2904	1.5281	–2.0835	–0.1573
6	0.1303	3.8622	–0.2928	–1.6097	0.1999
7	1.7123	0.4714	–2.8256	0.7500	–0.0751
8	3.6935	–0.7022	0.0833	0.7412	–0.1437
9	–1.4085	–0.2964	–3.0117	0.2228	0.2312

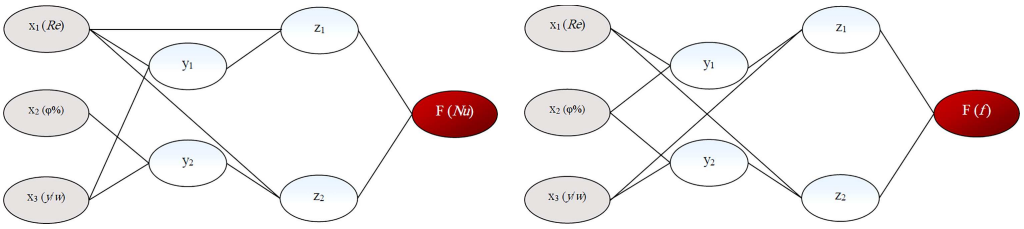

(a) (b)

FIG. 4: Structure of the developed GMDH-type neural networks for (a) Nu and (b) f model

TABLE 6: Polynomial equations related to the GMDH-ANN for Nu prediction

$y_1 = 156.178 + 0.01064x_1 - 61.226x_3 - 0.00092x_1x_3 + 3.04 \times 10^{-8}x_1^2 + 7.1619x_3^2$
$y_2 = 324.90 + 52.036x_2 - 80.2288x_3 - 8.6371x_2x_3 + 56.933x_2^2 + 7.6199x_3^2$
$z_1 = 5.1520 + 0.73710y_1 + 0.00196x_1 - 3.24 \times 10^{-5}y_1x_1 + 0.00241y_1^2 - 1.00 \times 10^{-7}x_1^2$
$z_2 = 3.8159 - 0.19583y_2 + 0.00127x_1 + 4.26 \times 10^{-5}y_2x_1 + 0.00014y_2^2 - 2.11 \times 10^{-9}x_1^2$
$F = \mathrm{Nu} = 0.71297 - 0.09395z_1 + 1.0847z_2 + 0.01683z_1z_2 - 0.00820z_1^2 - 0.00855z_2^2$

used to obtain the best correlation constants. After using the experimental data, the following equation achieves for Nu prediction:

$$\mathrm{Nu} = 0.133\mathrm{Re}^{0.78}\left(\frac{y}{w}\right)^{-0.46}(1+\phi)^{0.424} \tag{31}$$

The calculated MRE and MSE of the above correlation are 2.24% and 14.67, respectively. In addition, a correlation related to the f was proposed as follows:

$$f = 1.902\mathrm{Re}^{-0.223}\left(\frac{y}{w}\right)^{-0.312}(1+\phi)^{0.811} \tag{32}$$

The MRE and MSE of 2.75% and 3.8×10^{-5} were calculated for the f correlation. The ranges of the parameters used in Eqs. (31) and (32) were reported in Table 1.

TABLE 7: Polynomial equations related to the GMDH-ANN for f prediction

$y_1 = 0.21712 - 6.11 \times 10^{-6}x_1 + 0.08929x_2 - 8.39 \times 10^{-7}x_1x_2 + 1.14 \times 10^{-10}x_1^2 + 0.05475x_2^2$
$y_2 = 0.30877 + 0.08325x_2 - 0.06738x_3 + 0.00716x_2x_3 + 5.08 \times 10^{-3}x_2^2 + 0.00631x_3^2$
$z_1 = 0.19796 + 0.648610y_1 - 0.07296x_3 - 0.01205y_1x_3 + 1.0807y_1^2 + 0.00744x_3^2$
$z_2 = 0.11478 + 0.25988y_2 - 4.06 \times 10^{-6}x_1 - 1.85 \times 10^{-5}y_2x_1 + 2.8152y_2^2 + 1.46 \times 10^{-10}x_1^2$
$F = f = 0.00088 + 4.1490z_1 - 3.1516z_2 + 123.33z_1z_2 - 71.447z_1^2 - 51.877z_2^2$

3.4 Compare the Accuracy of the Models

The prediction performance of the investigated models was compared. Table 8 reports the deviation values of the MLP and GMDH neural networks and GA-based correlations for predicting Nu and f. The errors related to the prediction of training, testing, and overall data points are reported in the table. In general, the performances of the three models are acceptable. The neural networks appear more accurate in comparison with the GA correlations. However, the results indicate the superior performance of the MLP neural network, especially about the prediction of f.

3.5 GA Multiobjective Optimization

The higher heat transfer coefficients for the investigated heat exchanger are associated with higher f and the importance of optimization is determined. The global optimal results can be obtained using the GA procedure after searching for a part of the search space. The operating parameters including Re, y/w, and φ according to the studied ranges (reported in Table 1) were optimized using GA multiobjective optimization to achieve maximum Nu and minimum f. For this reason, the objective functions of OF_1 and OF_2 [Eqs. (28) and (29)] were introduced to the GA. In this study, the more accurate predictive model, MLP-ANN, was used to calculate the objective function values, and the GA multiobjective optimization is adopted in searching for optimum parameters based on the estimated fitness values. The purpose of the used optimization

TABLE 8: Prediction accuracy of the employed models

Model	Stage	Data points	Nu	—	f	—
			MRE (%)	MSE	MRE (%)	MSE
MLP-ANN	Training	88	0.169	0.086	0.040	1.21×10^{-8}
	Testing	44	0.250	0.162	0.112	9.65×10^{-8}
	Overall	132	0.196	0.111	0.063	3.97×10^{-8}
GMDH-ANN	Training	88	0.687	1.865	1.268	1.16×10^{-5}
	Testing	44	0.780	3.013	1.390	1.46×10^{-5}
	Overall	132	0.718	2.248	1.309	1.26×10^{-5}
GA-based correlation [Eqs. (31) and (32)]	—	—	2.243	14.67	2.747	3.80×10^{-5}

method is to achieve a trade-off between the heat transfer coefficient and friction characteristic. The optimum answers (Pareto set) of the system generated by the GA multiobjective optimization and the corresponding Nu and f were shown in Figs. 5(a) and 5(b), respectively. Each point in the Pareto set presented two values of the objectives that are a global optimal result and there is no point superior to the other. The conflict changes of the target variables prove the need for optimization.

Three desired parameters for optimization (Re, y/w, and φ) related to the Pareto set points were shown in Fig. 6. As seen in Fig. 6(a), the obtained optimum values of Re were approximately constant at its upper limit due to ideal values of Nu and f in higher values of Re. Figure 6(b) illustrates the optimal values of the y/w in terms of Nu. As expected, the y/w decreases with increasing Nu in higher values of y/w. However, there is a constant trend for y/w at its

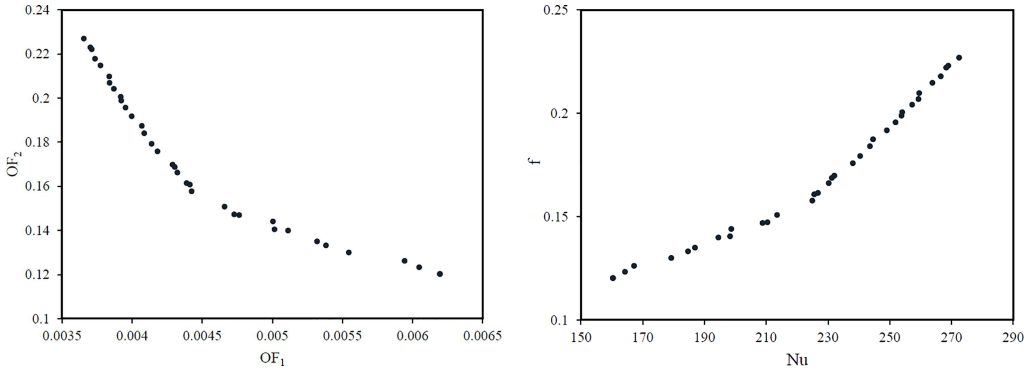

FIG. 5: (a) The obtained Pareto set of the objective functions and (b) corresponding Nu and f values

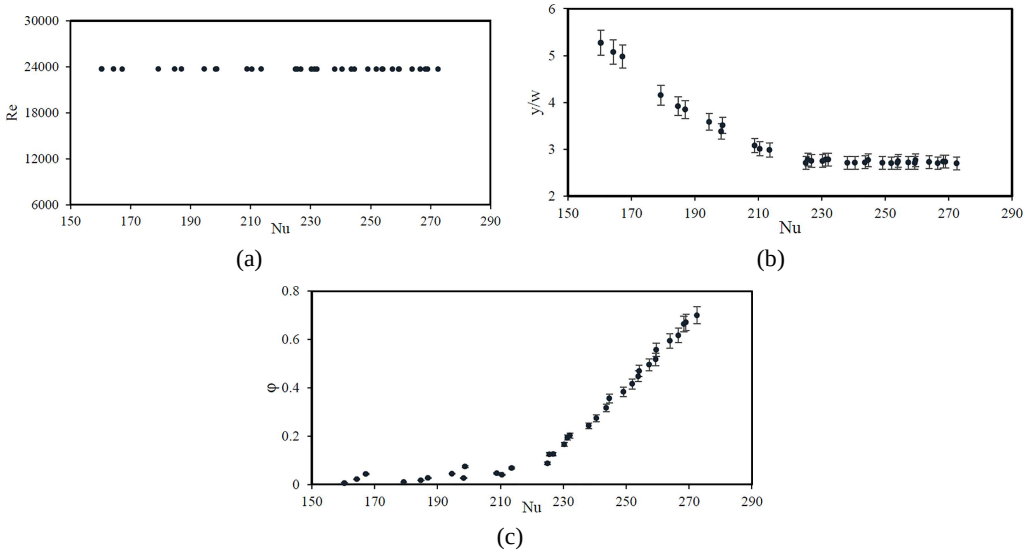

FIG. 6: The values of the operating variables (Re, y/w, and φ) related to the points on the Pareto set

low values versus increasing Nu. The optimum values of the φ in terms of Nu were shown in Fig. 6(c). The figure indicates that the nanomaterial is more effective at lower concentrations.

The optimization results indicate that higher Re values lead to ideal Nu and f. Therefore, design parameters have to be determined in a given Re. The obtained Pareto set at different Re is shown in Fig. 7. The figure shows the significant effect of the Re on the optimum answers. In addition, Table 9 reports some of the selected optimum answers and related Nu and f at various Re. More geometrical parameters can be obtained using the GA multiobjective optimization method for different Re. Each value reported in the table was obtained based on a trade-off between Nu and f. The designing of the heat exchanger and selecting the design parameters (Re, y/w, and φ) was performed based on the importance of Nu and f.

4. CONCLUSIONS

This study introduced and compared three well-known ANN techniques including MLP, GMDH, and GA. The heat exchanger, which benefits three HTE options (tube insert, corrugated tube, and nanofluid), has been modeled successfully by these techniques to estimate the thermal and flow characteristics. The Nu and f were modeled as functions of mainly influencing parameters including volume fraction of nanoparticle (φ), twist ratios of twisted tape (y/w), and Re. The MLP-ANNs with three layers and eight and nine neurons in the hidden layer were proposed for Nu and f prediction, respectively. The polynomial equations related to the two developed GMDH-ANNs were presented. In addition, two GA-based correlations in the form of the power-law equation were developed for predicting the target variables. Evaluating the prediction accuracy of the model outputs indicates that all three approaches are precise and reliable. However, the lower deviation values related to the MLP-ANN indicate this technique is proper to predict target variables in the investigated heat exchanger.

The simultaneous use of twisted tape and nanofluid increases the convective heat transfer and pressure drop. The increasing CuO concentration and twisted ratio of twisted tape lead to an increase in the Nu and f. The enhancement of the convective heat transfer is a useful effect but increasing the pressure drop follows with more needed pumping power. Therefore

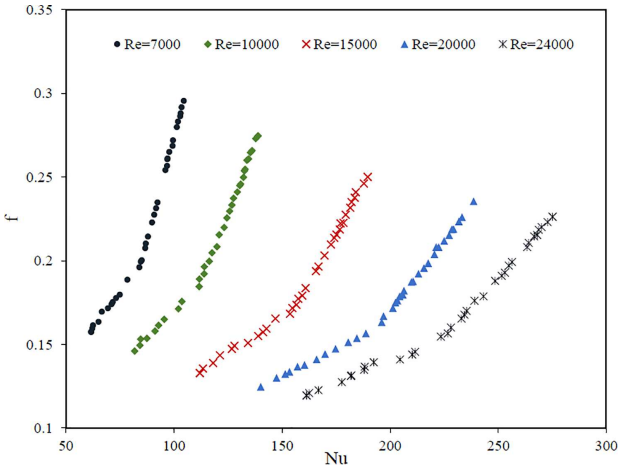

FIG. 7: Optimum answers (Pareto set) in different Re

TABLE 9: A selection of the optimum results

Re	φ (%)	y/w	Nu	f
7000	0.0030	5.29	61.78	0.1574
7000	0.0126	3.68	73.27	0.1776
7000	0.0940	2.74	86.80	0.2075
7000	0.2286	2.75	90.91	0.2275
7000	0.4124	2.78	96.08	0.2541
7000	0.6088	2.75	101.91	0.2831
7000	0.6873	2.72	104.65	0.2955
10000	0.0074	5.27	81.87	0.1461
10000	0.0160	4.19	91.28	0.1580
10000	0.0403	3.88	95.57	0.1650
10000	0.1543	2.91	114.06	0.1964
10000	0.3423	2.76	124.49	0.2256
10000	0.6042	2.78	133.79	0.2600
10000	0.6940	2.74	137.84	0.2730
15000	0.0033	5.28	112.01	0.1329
15000	0.0469	4.62	121.32	0.1435
15000	0.0110	3.59	134.27	0.1509
15000	0.1193	2.79	157.49	0.1773
15000	0.2418	2.75	165.68	0.1938
15000	0.4703	2.73	178.46	0.2226
15000	0.6959	2.73	189.70	0.2501
20000	0.0029	5.29	140.13	0.1246
20000	0.0210	3.72	166.03	0.1411
20000	0.0482	3.02	184.68	0.1538
20000	0.0873	2.74	196.12	0.1633
20000	0.2944	2.76	210.63	0.1877
20000	0.4697	2.75	222.48	0.2082
20000	0.6997	2.70	238.68	0.2356
24000	0.0020	5.29	161.36	0.1195
24000	0.0281	4.17	182.13	0.1315
24000	0.0110	3.19	204.62	0.1410
24000	0.0803	2.71	226.75	0.1565
24000	0.1591	2.72	233.03	0.1654
24000	0.3815	2.71	251.67	0.1911
24000	0.5641	2.73	264.19	0.2107
24000	0.7000	2.70	275.23	0.2263

the multiobjective optimization is essential for the investigated system. The optimum operating parameters of the investigated heat exchanger that led to a trade-off between heat transfer and friction characteristics were proposed using the GA multiobjective optimization. Each value of the operating conditions can be selected according to the project purpose.

REFERENCES

Abdollahi-Moghaddam, M., Motahari, K., and Rezaei, A., Performance Characteristics of Low Concentrations of CuO/Water Nanofluids Flowing through Horizontal Tube for Energy Efficiency Purposes: An Experimental Study and ANN Modeling, *J. Mol. Liq.*, vol. **271**, pp. 342–352, 2018.

Ahmadi, M., Ahmadi, M.-A., Mehrpooya, M., and Rosen, M., Using GMDH Neural Networks to Model the Power and Torque of a Stirling Engine, *Sustainability*, vol. **7**, no. 2, pp. 2243–2255, 2015.

Al-Rashed, A.A., Shahsavar, A., Rasooli, O., Moghimi, M., Karimipour, A., and Tran, M.D., Numerical Assessment into the Hydrothermal and Entropy Generation Characteristics of Biological Water-Silver Nano-Fluid in a Wavy Walled Microchannel Heat Sink, *Int. J. Heat Mass Transf.*, vol. **104**, pp. 118–126, 2019.

Ali, J.M., Hussain, M.A., Tade, M.O., and Zhang, J., Artificial Intelligence Techniques Applied as Estimator in Chemical Process Systems—A Literature Survey, *Expert Syst. Appl.*, vol. **42**, no. 14, pp. 5915–5931, 2015.

Baghban, A., Kahani, M., Nazari, M.A., Ahmadi, M.H., and Yan, W.-M., Sensitivity Analysis and Application of Machine Learning Methods to Predict the Heat Transfer Performance of CNT/Water Nanofluid Flows through Coils, *Int. J. Heat Mass Transf.*, vol. **128**, pp. 825–835, 2019.

Bahiraei, M. and Heshmatian, S., Electronics Cooling with Nanofluids: A Critical Review, *Energy Convers. Manag.*, vol. **172**, pp. 438–456, 2018.

Beigzadeh, R., Rahimi, M., Parvizi, M., and Eiamsa-ard, S., Application of ANN and GA for the Prediction and Optimization of Thermal and Flow Characteristics in a Rectangular Channel Fitted with Twisted Tape Vortex Generators, *Numer. Heat Tr. A-Appl.*, vol. **65**, no. 2, pp. 186–199, 2014.

Boulahia, Z., Wakif, A., Chamkha, A.J., and Sehaqui, R., Numerical Study of Natural and Mixed Convection in a Square Cavity Filled by a Cu–Water Nanofluid with Circular Heating and Cooling Cylinders, *Mech. Ind.*, vol. **18**, no. 502, 2017.

Einstein, A., Berichtigung zu Meiner Arbeit: Eine neue Bestimmung der Moleküldimensionen, *Ann. Phys.*, vol. **339**, pp. 591–592, 1911.

Fard, A.M., Mirjalily, S.A.A., and Ahrar, A.J., Influence of Carbon Nanotubes on Pressure Drop and Heat Transfer Rate of Water in Helically Coiled Tubes, *J. Enhanced Heat Transf.*, vol. **26**, no. 3, pp. 217–233, 2019.

Fujimoto, K. and Nakabayashi, S., Applying GMDH Algorithm to Extract Rules from Examples, *Syst. Anal. Model. Simulat.*, vol. **43**, no. 10, pp. 1311–1319, 2003.

Ghahdarijani, A.M., Hormozi, F., and Asl, A.H., Convective Heat Transfer and Pressure Drop Study on Nanofluids in Double-Walled Reactor by Developing an Optimal Multilayer Perceptron Artificial Neural Network, *Int. Commun. Heat Mass*, vol. **84**, pp. 11–19, 2017.

Guo, Z., A Review on Heat Transfer Enhancement with Nanofluids, *J. Enhanced Heat Transf.*, vol. **27**, no. 1, pp. 1–70, 2020. DOI: 10.1615/JEnhHeatTransf.2019031575

Ivakhnenko, A.G., Polynomial Theory of Complex Systems, *IEEE Trans. Syst. Man. Cybern.*, vol. **1**, pp. 364–378, 1971.

Izadi, S., Armaghani, T., Ghasemiasl, R., Chamkha, A.J., and Molana, M., A Comprehensive Review on Mixed Convection of Nanofluids in Various Shapes of Enclosures, *Powder Technol.*, vol. **343**, pp. 880–907, 2019.

Konak, A., Coit, D.W., and Smith, A.E., Multi-Objective Optimization Using Genetic Algorithms: A Tutorial, *Reliab. Eng. Syst. Safe.*, vol. **91**, no. 9, pp. 992–1007, 2006.

Mohanraj, M., Jayaraj, S., and Muraleedharan, C., Applications of Artificial Neural Networks for Thermal Analysis of Heat Exchangers—A Review, *Int. J. Therm. Sci.*, vol. **90**, pp. 150–172, 2015.

Molana, M., On the Nanofluids Application in the Automotive Radiator to Reach the Enhanced Thermal

Performance: A Review, *Am J. Heat Mass Transf.*, vol. **4**, no. 4, pp. 168–187, 2017.

Nagaraj, P., A Review of Experimental and Numerical Investigation on the Heat Transfer in Micro-Channel Heat Exchanger for Various Nano Fluids, *Recent Trends Fluid Mech.*, vol. **5**, pp. 1–7, 2019.

Nandakrishnan, S., Deepu, M., and Shine, S., Numerical Investigation of Heat-Transfer Enhancement in a Dimpled Diverging Microchannel with Al_2O_3–Water Nanofluid, *J. Enhanced Heat Transf.*, vol. **25**, nos. 4-5, pp. 347–365, 2018.

Nasr, M.J., Khalaj, A.H., and Mozaffari, S., Modeling of Heat Transfer Enhancement by Wire Coil Inserts Using Artificial Neural Network Analysis, *Appl. Therm. Eng.*, vol. **30**, nos. 4-5, pp. 143–151, 2010.

Nasr, M.R.J. and Khalaj, A.H., Heat Transfer Coefficient and Friction Factor Prediction of Corrugated Tubes Combined with Twisted Tape Inserts Using Artificial Neural Network, *Heat Transf. Eng.*, vol. **31**, no. 1, pp. 59–69, 2010.

Pak, B.C. and Cho, Y.I., Hydrodynamic and Heat Transfer Study of Dispersed Fluids with Submicron Metallic Oxide Particles, *Exp. Heat Transf. Int. J.*, vol. **11**, no. 2, pp. 151–170, 1998.

Pal, S.K. and Bhattacharyya, S., Enhanced Heat Transfer of Cu-Water Nanofluid in a Channel with Wall Mounted Blunt Ribs, *J. Enhanced Heat Transf.*, vol. **25**, no. 1, pp. 61–78, 2018.

Piriyarungrod, N., Kumar, M., Thianpong, C., Pimsarn, M., Chuwattanakul, V., and Eiamsa-ard, S., Intensification of Thermo-Hydraulic Performance in Heat Exchanger Tube Inserted with Multiple Twisted-Tapes, *Appl. Therm. Eng.*, vol. **136**, pp. 516–530, 2018.

Sanaye, S. and Dehghandokht, M., Modeling and Multi-Objective Optimization of Parallel Flow Condenser Using Evolutionary Algorithm, *Appl. Energy*, vol. **88**, no. 5, pp. 1568–1577, 2011.

Shabanian, S., Rahimi, M., Shahhosseini, M., and Alsairafi, A., CFD and Experimental Studies on Heat Transfer Enhancement in an Air Cooler Equipped with Different Tube Inserts, *Int. Commun. Heat Mass*, vol. **38**, no. 3, pp. 383–390, 2011.

Vajjha, R.S., Das, D.K., and Namburu, P.K., Numerical Study of Fluid Dynamic and Heat Transfer Performance of Al_2O_3 and CuO Nanofluids in the Flat Tubes of a Radiator, *Int. J. Heat Fluid Flow*, vol. **31**, no. 4, pp. 613–621, 2010.

Wongcharee, K. and Eiamsa-ard, S., Heat Transfer Enhancement by Using CuO/Water Nanofluid in Corrugated Tube Equipped with Twisted Tape, *Int. Commun. Heat Mass*, vol. **39**, no. 2, pp. 251–257, 2012.

Zheng, N., Liu, P., Wang, X., Shan, F., Liu, Z., and Liu, W., Numerical Simulation and Optimization of Heat Transfer Enhancement in a Heat Exchanger Tube Fitted with Vortex Rod Inserts, *Appl. Therm. Eng.*, vol. **123**, pp. 471–484, 2017.

Zimparov, V., Enhancement of Heat Transfer by a Combination of Three-Start Spirally Corrugated Tubes with a Twisted Tape, *Int. J. Heat Mass Transf.*, vol. **44**, no. 3, pp. 551–574, 2001.

Zimparov, V., Prediction of Friction Factors and Heat Transfer Coefficients for Turbulent Flow in Corrugated Tubes Combined with Twisted Tape Inserts. Part 1: Friction Factors, *Int. J. Heat Mass Transf.*, vol. **47**, no. 3, pp. 589–599, 2004.

Zimparov, V., Prediction of Friction Factors and Heat Transfer Coefficients for Turbulent Flow in Corrugated Tubes Combined with Twisted Tape Inserts. Part 2: Heat Transfer Coefficients, *Int. J. Heat Mass Transf.*, vol. **47**, pp. 385–393, 2004.